

# Hydrodynamic permeability of dendritic crystals

Thomas Zielinski<sup>\*1</sup>, I. Marcel Nkenfack<sup>\*\*2</sup>, Miha Zaloznik<sup>\*\*\*3</sup>, and J. S. Kroll-Rabotin<sup>†3</sup>

<sup>1</sup>*École des Mines de Nancy, France*

<sup>2</sup>*Master Énergie, Université de Lorraine, Nancy, France*

<sup>3</sup>*Institut Jean Lamour, Université de Lorraine, Nancy, France*

June 11, 2022

## Abstract

In a metallurgical process, the chemical homogeneity of alloys is controlled by the solidification of dendritic crystals transported in the liquid flow. Hence, the understanding of the dynamics governing these complex objects is of paramount interest. Scientific literature provides models of drag force acting on dendrites which rely on strong morphological simplifications of the dendrite geometry. In this work, dendrites obtained from simulations of solidification have been studied without further morphological approximations. Results have shown that dendrite dynamics have been modeled by analogy with spheres. Moreover, the distribution in space of the force acting on dendrites has also been studied. A distribution of permeability has then been established using Darcy's law.

## Nomenclature

$\alpha$	Form factor for each dendrites.	$L_{dendrite}$	Number of mesh grids representing the dendrites in the simulation domain.
$\chi$	Confinement factor for the spheres.	$L_{dendrite}^{PF}$	Number of mesh grids representing the dendrites in the Phase Field.
$\Delta p$	Pressure jump applied in a plane normal to the flow direction.	$N^*$	Dimensionless factor representing the averaging compared to the size of the primary branch of dendrites.
$\langle \bar{v} \rangle$	Average velocity field.	$Q$	Volume flow rate.
$\mu$	Dynamic viscosity of the fluid.	$v$	Velocity of the flow.
$\nu$	Kinematic viscosity of the fluid.	$X_L$	Binary number associated to each mesh grid which equals to 1 for the liquid and 0 for the solid.
$\bar{K}$	Tensor of permeability.		
$F_{drag}$	Drag force applied on the surface of an object.		
$f_{vol}$	Spatial distribution of the force applied on the surface of the object.		
$\rho$	Volumic mass of the metal alloy		
$D_{sphere}$	Diameter of the sphere.		
$g_L$	Liquid fraction.		
$h$	Reduction factor for the importation of the dendrites.		
$k$	Confinement coefficient for the spheres.		
$k'$	Confinement coefficient for the dendrites.		
$l_y$	Number of mesh grids in the simulation domain along the y axis.		

## 1 Introduction

During the solidification of a metal alloy in order to obtain metal ingots that are then shaped as a material, a branched structure called dendrites appears. During their growth, two types of dendrites can emerge : the equiaxed dendrites or the columnar dendrites. In order to control the chemical homogeneity of the material, and thus their mechanical properties, the dynamics of these dendrites and their interactions with the liquid have to be carefully studied. The dynamics of the spheres at low Reynolds number is well-known. Indeed, the drag force can be expressed as follows :

$$\overline{F_{drag}} = 3\pi\rho\nu D_{sphere}\bar{v} \quad (1)$$

The dynamics of the dendrites is then obtained by analogy with the spheres introducing a shape factor  $\alpha$ , which is unique for each geometry of dendrite, in order to take into consideration the differences between a sphere and a

\*E-mail: thomas.zielinski6@etu.univ-lorraine.fr

\*\*E-mail: isibert-marcel.nkenfack9@etu.univ-lorraine.fr

\*\*\*Corresponding author: miha.zaloznik@univ-lorraine.fr

†E-mail: jean-sebastien.kroll-rabotin@univ-lorraine.fr

dendrite. Besides, the various values of  $\alpha$  have been calculated depending on the different geometries of dendrites, some examples of which are presented in Figure 1, in order to find a model of drag force expressed as follows :

$$\overline{F_{drag}} = 3\pi\rho\nu L_{dendrite} \alpha \bar{v} \quad (2)$$

To this day, certain theoretical models of drag force applied on the surface of the dendrites have been developed. For instance, de Groh III et al. [1] studied the effect of the shape of dendrites on their drag but significantly approximated the dendrite geometry. To overcome this limitation, this study focuses on real dendrites obtained from phase field simulations of solidification [2]. Numerical simulations using the Lattice Boltzmann Method (LBM) have been implemented in order to quantify  $\alpha$  and to study in depth the drag force applied on the surface of the dendrites. This study does not limit itself with the single value of the drag force but also highlights its distribution on the surface of the dendrites and models it through a distribution of permeability in the dendrite envelope.

## 2 Definition of the problem

### 2.1 Drag force

Considering the fact that the dynamics of the spheres are well known, dendrites' dynamics can be obtained by analogy with the spheres.

The force that applies on a periodic lattice of objects within a flow depends on the size of the mesh of the lattice characterized by a confinement. For objects like spheres and dendrites, this confinement can be quantified by the coefficient  $\chi$ , which represents the length of this object compared to the distance between them. This confinement coefficient can be determined as follows :

$$\chi = \frac{\text{Length of the object}}{\text{Distance between the objects}} \quad (3)$$

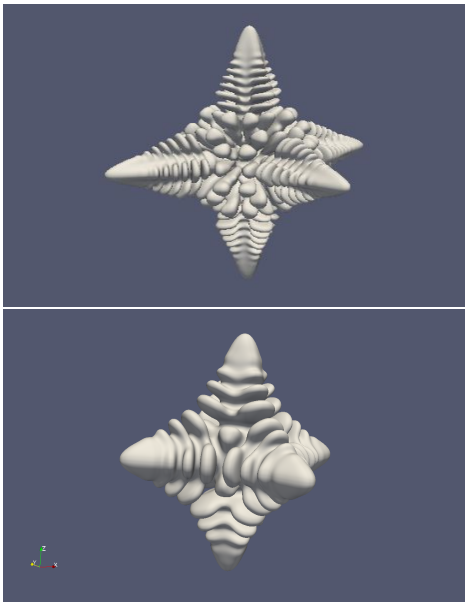


**Figure 1.** Dendrite obtained from phase field simulations in various conditions of solidification [2].

To account for this confinement, a factor  $k$  depending on  $\chi$  can be introduced in the expression of the drag force. However, this coefficient  $k$  also depends on morphological properties. Different confinement coefficients  $k$  for the spheres and  $k'$  for the dendrites must then be introduced in equations (1) and (2).

$$\overline{F_{drag sphere}} = 3\pi\rho\nu D_{sphere} \bar{v} k \quad (4)$$

$$\overline{F_{drag dendrite}} = 3\pi\rho\nu L_{dendrite} \alpha \bar{v} k' \quad (5)$$

Sangani and Acrivos [3] have calculated the confinement coefficient  $k$  for spheres based on Taylor expansion of the analytical solution and provided the coefficients  $\beta_i$  of the Taylor series.

$$k(\chi) = \sum_{i=0}^{30} \beta_i \chi^i \quad (6)$$

### 2.2 Spatial distribution of force

Once the dynamics of the dendrites obtained, a spatial distribution of the force around the dendrites is needed in order to characterize the flow near the dendrites. It is proposed to consider the dendrite as a porous medium. It can then be characterized by an envelope [1] and a permeability due to the presence of their secondary branches.

A volume distribution of the drag force  $\overline{f_{vol}}$  is obtained and can be characterised as the exchange of momentum between the liquid phase and the solid phase. A finer model based on a permeability inside the dendrites can then be established by analogy with Darcy's Law for porous flows and averaging the volumetric distribution of the drag force.

$$\langle \bar{v}_L \rangle^L = \frac{-1}{\mu} \overline{\bar{K}} \cdot \nabla \langle p_L \rangle^L \quad (7)$$

$$\text{where } \langle \bar{v}_L \rangle^L = \frac{\langle \bar{v}_L \rangle}{g_L} \quad (8)$$

$$\text{where } \overline{\nabla} \langle p_L \rangle^L = \overline{\nabla} \frac{\langle p_L \rangle}{g_L} \quad (9)$$

In this equation,  $\langle \bar{v}_L \rangle^L$  and  $\langle p_L \rangle^L$  represent respectively the averaged velocity and pressure in the liquid in a representative volume element (RVE). The averaged fields are calculated based on the results of numerical simulations. As  $\langle \bar{v}_L \rangle^L$  and  $\langle p_L \rangle^L$  depend on the size of the RVE, the relevant size of the RVE has also been investigated. Using the variable  $X_L$  which is a binary value equaling 1 in the liquid and 0 in the solid,  $\langle \bar{v}_L \rangle^L$  and  $\langle p_L \rangle^L$  can be calculated as follows :

$$\langle \bar{v}_L \rangle^L = \frac{1}{V_L} \int_{RVE} \bar{v} \cdot X_L dV \quad (10)$$

$$\langle p_L \rangle^L = \frac{1}{V_L} \int_{RVE} p \cdot X_L dV \quad (11)$$

The average is characterized by the variable  $N^*$  representing the size of a representative elementary volume. RVE of cubic shapes are used.  $N^*$  is thus defined as :

$$N^* = \frac{2 \times \text{Length of the RVE edge}}{\text{Length of the object}} \quad (12)$$

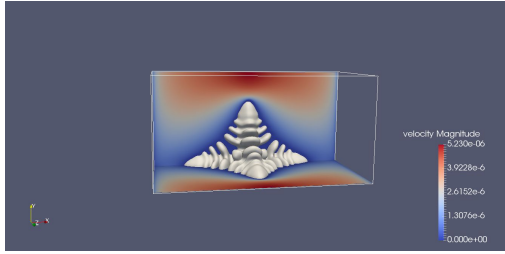


**Figure 2.** Simulation domain for the dendrites

In order to have an order of magnitude, Martin de Bazelaire [4] had found that the proper value of  $N^*$  is between 0.12 and 0.19.

Making the assumption that the tensor of permeability  $\bar{\bar{K}}$  is diagonal, it can thus be expressed as follows :

$$\bar{\bar{K}} = \begin{pmatrix} k_{xx} & 0 & 0 \\ 0 & k_{yy} & 0 \\ 0 & 0 & k_{zz} \end{pmatrix}$$

In this study, only the first component  $k_{xx}$  of the tensor is studied because it represents the component in the direction of the flow along the x axis. The component  $k_{xx}$  can then be calculated as follows :

$$k_{xx} = -\mu \frac{(\langle \bar{v}_L \rangle^L)_x}{(\nabla \langle p_L \rangle^L)_x} \quad (13)$$

As the pressure is not easily determinable within the dendrites, a variation of Darcy's Law has been used, in which the pressure gradient is estimated by a local volume force  $f_{vol}$  calculated by averaging the force distribution on the surface of dendrites.

$$\langle \bar{v}_L \rangle^L = \frac{-1}{\mu} \bar{\bar{K}} \cdot \langle f_{vol} \rangle \quad (14)$$

The permeability then becomes :

$$k_{xx} = -\mu \frac{(\langle \bar{v}_L \rangle^L)_x}{\langle f_{vol} \rangle_x} \quad (15)$$

The evolution of the coefficient  $k_{xx}$  in terms of the size  $N^*$  of the representative elementary volume (RVE) is used as a criterion to properly chose the RVE size.

### 3 Material and methods

#### 3.1 Simulation using a Lattice Boltzmann Method

In order to quantify the liquid-solid interaction and to study the liquid flow around objects, the Lattice Boltzmann Method using a cubic and periodic simulation domain has been implemented [5]. Also known as LBM, this method solves the Navier-Stokes equations in the unsteady case in an incompressible flow thanks to the discretization of Boltzmann's equations in the velocity space. The flow within a cubic lattice of objects has been resolved by simulating a quarter of one object and using symmetry and periodicity as boundary conditions as shown in Figure 2 and 3. The

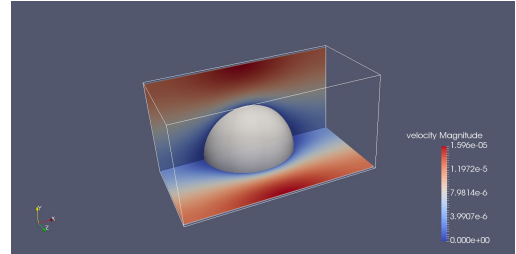


**Figure 3.** Simulation domain for the spheres

boundary condition to describe the surface of immersed objects is an interpolated bounce-back [6].

A pressure jump  $\Delta p$  is applied in a plane normal to the flow direction (x axis). In order to optimize the simulation time, only a quarter of a cubic domain was implemented. The rest of the dendrites or spheres and the fields of physical quantities are obtained by symmetry. The force applied on the immersed object is thus :

$$F_{drag} = 4\Delta p l_y^2 \quad (16)$$

where  $l_y$  is the length of the side of the simulation domain in the directions perpendicular to the flow.

In order to compare the results to the theory from Sangani and Acrivos [3], the simulations must have reached a steady state. Considering the fact that the flow is viscous ( $Re \ll 1$ ), the simulated time is scaled by the diffusion time. For the steady state to be reached in all simulations, simulated time has been fixed to at least fifteen times the diffusion time.

$$T = 15 \times \frac{l_y^2}{\nu} \quad (17)$$

#### 3.2 Validation of the method

In order to verify the correct implementation of the Lattice Boltzmann Method, the verification of a theory from Sangani and Acrivos [3] has been obtained in the case of spheres. For each simulation, the necessary number of mesh grids representing the spheres were higher than 25 in order to describe the spheres correctly while minimizing the simulation time. Besides, for high values of  $\chi$ , it was verified that there were at least 2 mesh grids between the spheres and the edge of the simulation domain. Combining equations (4) and (16), the confinement coefficient  $k$  is calculated as follows:

$$k_{calculated} = \frac{2\Delta p l_y^3}{3\pi\mu\chi Q} \quad (18)$$

In this equation, the flow rate  $Q$  was calculated using Paraview with the IntegerVariables filter applied on a slice as shown in Figure 4 using the formula :

$$Q = \int_{S_{slice}} v dS = v l_y^2 \quad (19)$$

In correlation with the results of Sangani and Acrivos [3], the evolution of the confinement coefficient  $k$  depending on various value of  $\chi$  was obtained as shown in Figure 5 and Figure 6.

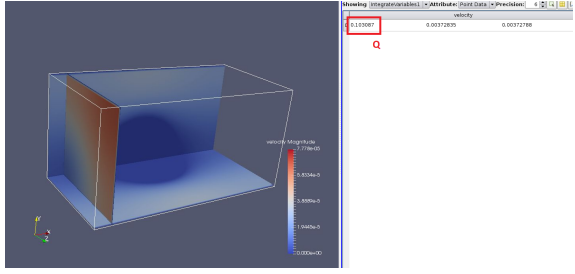


**Figure 4.** Calculation of the flow rate using Paraview

As shown in Table 1, the results are in agreement with the theory from Sangani and Acrivos [3] where the confinement coefficient tends towards 1 where  $\chi$  tends towards 0 and  $k$  increases when  $\chi$  increases, thus highlighting the growing impact of the confinement. For high values of  $\chi$ , a slightly bigger difference is noticed and highlights the limit of the theory of Sangani and Acrivos [3] that was already identified in their work. Finally, these results sheds light on the fact that the numerical method allows the description of immersed objects in confined lattices.

### 3.3 Mesh spacing for dendrites' simulation

The dendrites are initially represented in a phase field simulation of solidification described in D Tourret and Založník3 [2]. As the number of mesh grids necessary in the phase field is quite dense, it was decided to reduce the size of the mesh grids and thus its precision. To proceed with this transformation, a reduction factor  $h \in [0,1]$  was introduced in order to represent the reduction of precision between the phase field and the future simulation domain.

$$h = \frac{\Delta x_{LBM}}{\Delta x_{\text{Phase Field}}} \quad (20)$$

The confinement  $\chi$  is then calculated as follows :

$$\chi = \frac{h L_{\text{dendrite}}^{PF}}{2l_y} \quad (21)$$

To quantify the proper value of  $h$  that speeds up the simulation time and in order for the numerical simulations to stay correct, a study on the value of  $h$  has been conducted at Reynolds' number constant and  $\chi = 0.8$ . Choosing the value  $h = 1$  as the reference of precision, an error  $\epsilon$  depending on the value of  $h \in [0,1]$  was introduced.

$$\epsilon = 1 - \frac{F_{\text{drag calculated}}}{F_{\text{drag reference}}} \quad (22)$$

As shown in Figure 7, for a value of  $h = 0.25$ , the error is less than 1% and allows a significant reduction of the simulation time. In this way, the value  $h = 0.25$  is used in all the presented simulation results.

### 3.4 Permeability of dendrites as porous media

It is good to note that a permeability can be defined if it exists a relation between the slip velocity  $\bar{v}$  and the volume

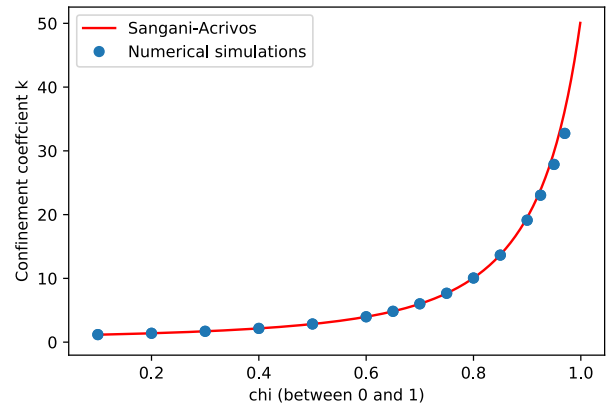


**Figure 5.** Evolution of the confinement coefficient  $k$  with confinement  $\chi$

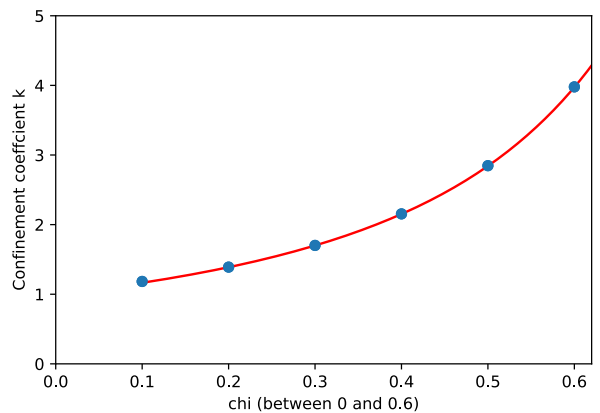


**Figure 6.** Zoom on the evolution of the confinement coefficient  $k$  for low values of  $\chi$

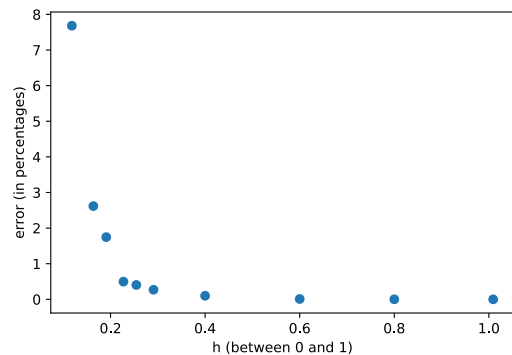


**Figure 7.** Evolution of the error in percentages with the value of  $h$

**Table 1.** Results for the spheres from the numerical simulations in order to compare the value  $k_{calculated}$  obtained from the simulations and the value  $k_{theory}$  obtained the theory from Sangani and Acrivos [3].

Evolution of the confinement coefficient k with $\chi$							
$\chi$	$l_y$	$T = 15 \frac{l_y^2}{\nu}$	Velocity	Reynolds	$k_{calculated}$	$\epsilon =  1 - \frac{k_{calculated}}{k_{theory}} $	
0.2	102	780300	4.714e-4	9.427e-2	1.4068	1.35%	
0.3	69	357075	1.740e-4	2.360e-2	1.7025	0.15%	
0.4	53	210675	7.427e-5	1.152e-2	2.1768	1.16%	
0.5	50	187500	4.474e-5	1.074e-2	2.8457	0.13%	
0.6	50	187500	2.667e-5	7.681e-3	3.9786	0.12%	
0.65	50	187500	2.026e-5	6.322e-3	4.8338	0.07%	
0.7	50	187500	1.513e-5	5.085e-3	6.0095	0.09%	
0.75	50	187500	1.108e-5	3.988e-3	7.6626	0.05%	
0.8	50	187500	7.913e-6	3.039e-3	10.0564	0.04%	
0.85	50	187500	5.487e-6	2.239e-3	13.6509	0.40%	
0.9	50	187500	2.542e-6	1.098e-3	19.1286	1.90%	
0.925	50	187500	2.986e-6	1.326e-3	23.0480	3.53%	
0.95	50	187500	1.868e-6	8.518e-4	27.8706	6.54%	
0.97	70	367500	2.840e-6	1.873e-3	32.7383	9.78%	

distribution of the drag force  $\overline{f_{vol}}$  that needs to be calculated.

To calculate a volume distribution of force, first the force distribution acting on a fluid on the surface of an object is calculated through the momentum exchange imposed in the interpolated bounce-back Bouzidi et al. [6]. Then, these exchanges of momentum are distributed on the lattice mesh nodes using a regularized Dirac distribution [7]. This gives a volume distribution of force  $\overline{f_{vol}}$  that can be averaged as the other fields.

Dendrite ID	alpha
Om25	0,843
Om20	0,833
Om15	0,823
Om10	0,775
Om05	0,763

**Table 2.** Values of alpha found for each geometry of dendrites.

## 4 Results and discussion

### 4.1 Dynamics of dendrites

Five different dendrites representing each various conditions of growth have been studied.

For each dendrite, the evolution of  $\alpha k'$  in terms of  $\chi$  was fitted with a polynomial of order 4 and only with even degrees was used in order to fit the points and determine the value of  $\alpha$ , the intercept. The polynomials were defined as follows :

$$P(\chi) = \alpha + A\chi^2 + B\chi^4 \quad (23)$$

The values of  $\alpha$ , A and B were obtained by least square regression. The results for  $\alpha$  are presented in Table 2. Figure 8, Figure 9 and Figure 10 highlight that there is a similar pattern for each geometries of dendrites with a slight vertical offset when the number of branches increases or decreases. Figure 11 allows the determination of the various values of  $\alpha$  depending on the geometries of the dendrites.

### 4.2 Hydrodynamic permeability

As shown from Figure 12 to Figure 15, the permeability calculated with equation (15) was first visualized in Paraview. Within a slice located at the plane of symmetry of the dendrite, the permeability was plotted with a scale ranging from 1 to 10000 where the yellow color represents an

undefined value. On this slice, the surface of the dendrite is represented in white. For different sizes of representative elementary volume, the permeability can be plotted and the averaging of the dendrite can then be visually compared to the original dendrite. The larger the representative elementary volume, the more the dendrite is averaged.

For small values of  $N^*$  represented in Figure 12, the dendrite is barely averaged and it is difficult to define a permeability. However, as shown in Figure 13, Figure 14 and Figure 15, a permeability is obtained and visualized for various increasing sizes of representative elementary volume. It can be inferred that a permeability appears as the size of the representative elementary volume  $N^*$  increases.

As this criteria is purely visual, it can be relevant to study the evolution of the permeability for every mesh nodes.

Then, from Figure 16 to Figure 21, the permeability was plotted in terms of the liquid fraction with logarithmic axes for different values of representative elementary volume  $N^*$ . For Figure 16, Figure 17 and Figure 18, the permeability is calculated with equation (13). Nevertheless, For Figure 19, Figure 20 and Figure 21, the permeability is calculated with equation (15). Every dots in black is associated to a mesh node of the simulation domain. For each mesh node, the permeability is plotted in terms of the liquid fraction for various sizes of representative elementary volume  $N^*$ . The dots in yellow represent the mesh nodes in the same slice visualized in Figure 12 to 15.

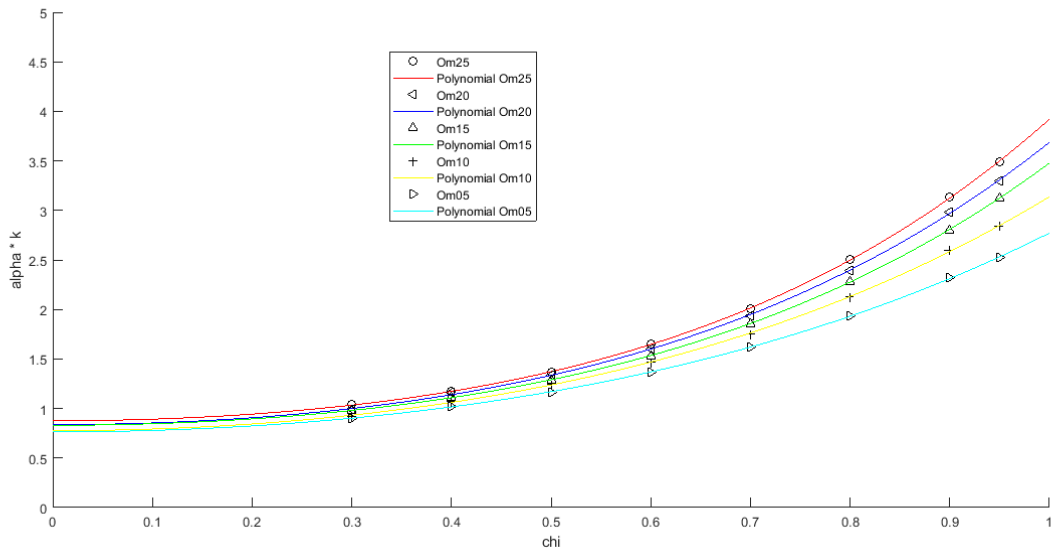


**Figure 8.** Evolution of the factor  $\alpha k'$  with  $\chi$  for different geometries of dendrites

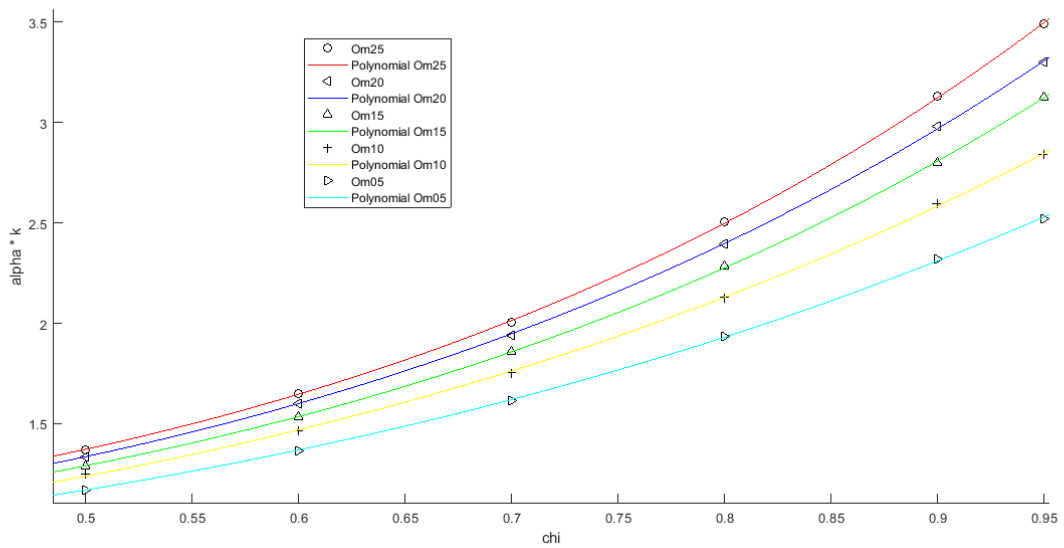


**Figure 9.** Zoom on the evolution of the factor  $\alpha k'$  with  $\chi$  for different geometries of dendrites

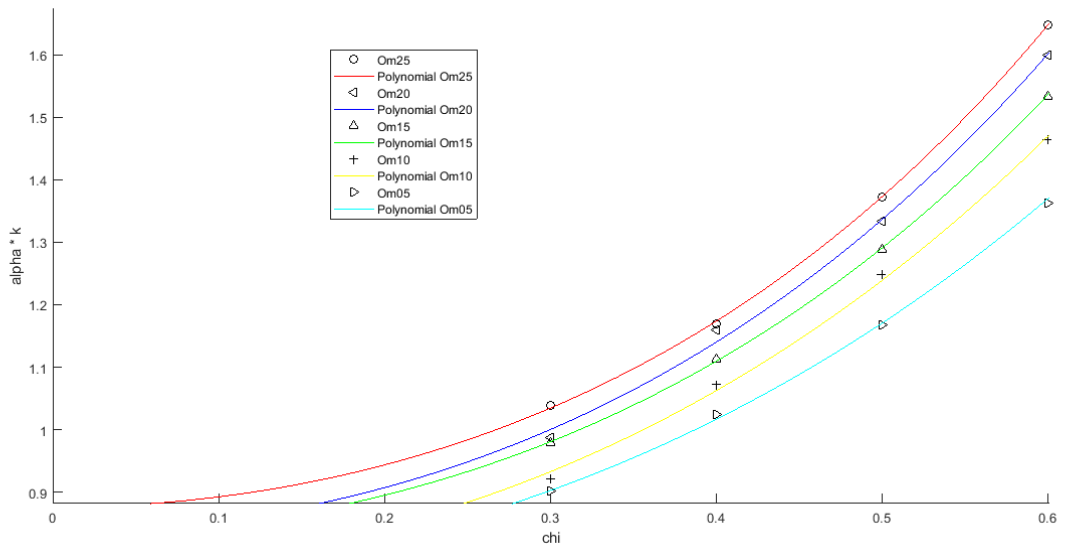


**Figure 10.** Zoom on the evolution of the factor  $\alpha k'$  with  $\chi$  for different geometries of dendrites

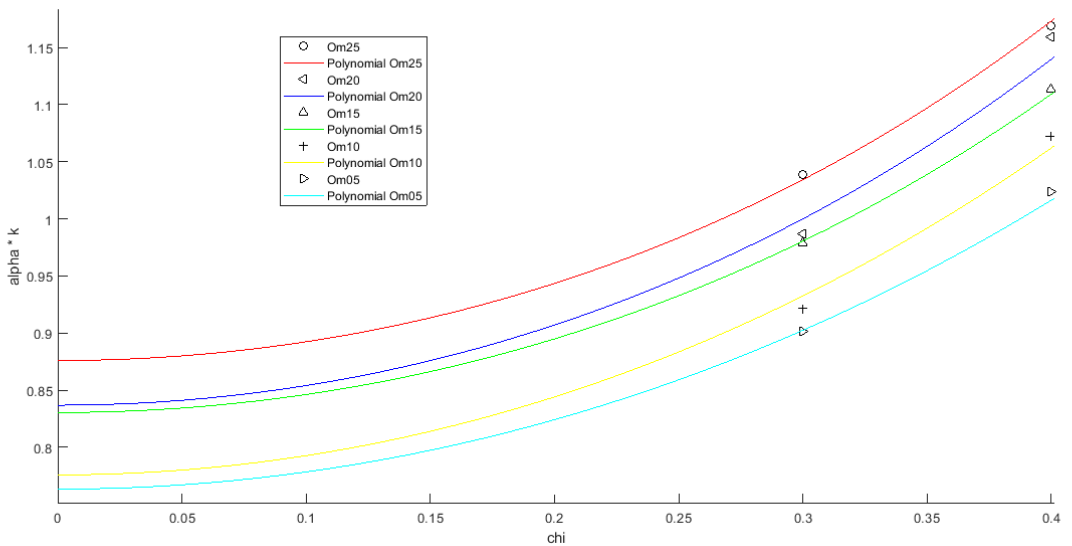


**Figure 11.** Zoom on the evolution of the factor  $\alpha k'$  with  $\chi$  for different geometries of dendrites

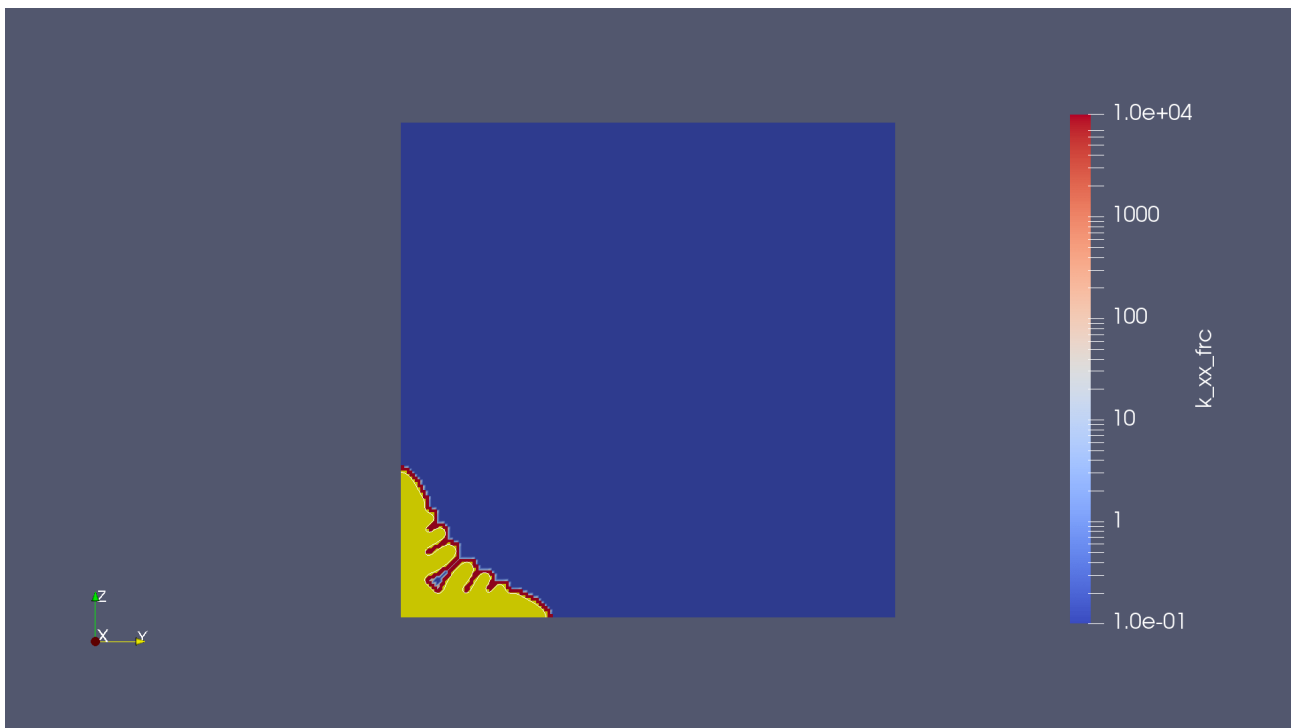


**Figure 12.** Visualisation in a slice in Paraview of  $k_{xx}$  obtained with the drag force for  $N^* = 0.009469$

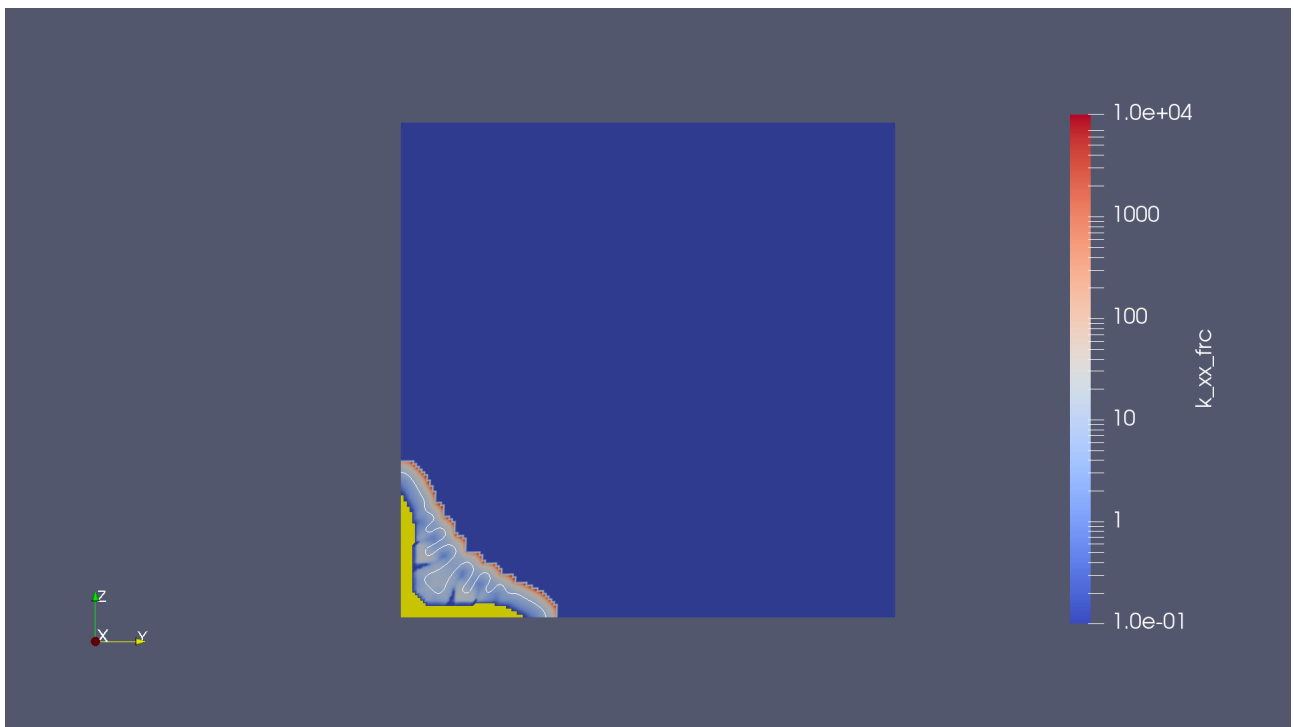


**Figure 13.** Visualisation in a slice in Paraview of  $k_{xx}$  obtained with the drag force for  $N^* = 0.0662$

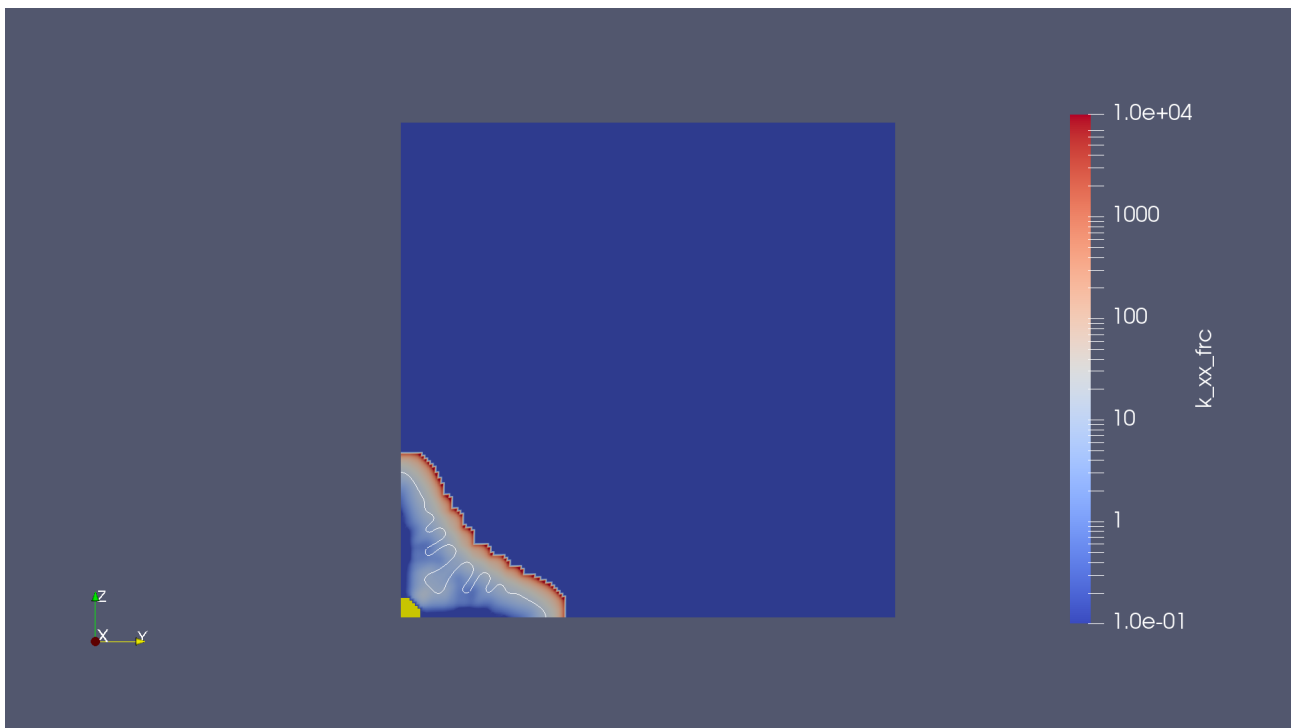


**Figure 14.** Visualisation in a slice in Paraview of  $k_{xx}$  obtained with the drag force for  $N^* = 0.1041$

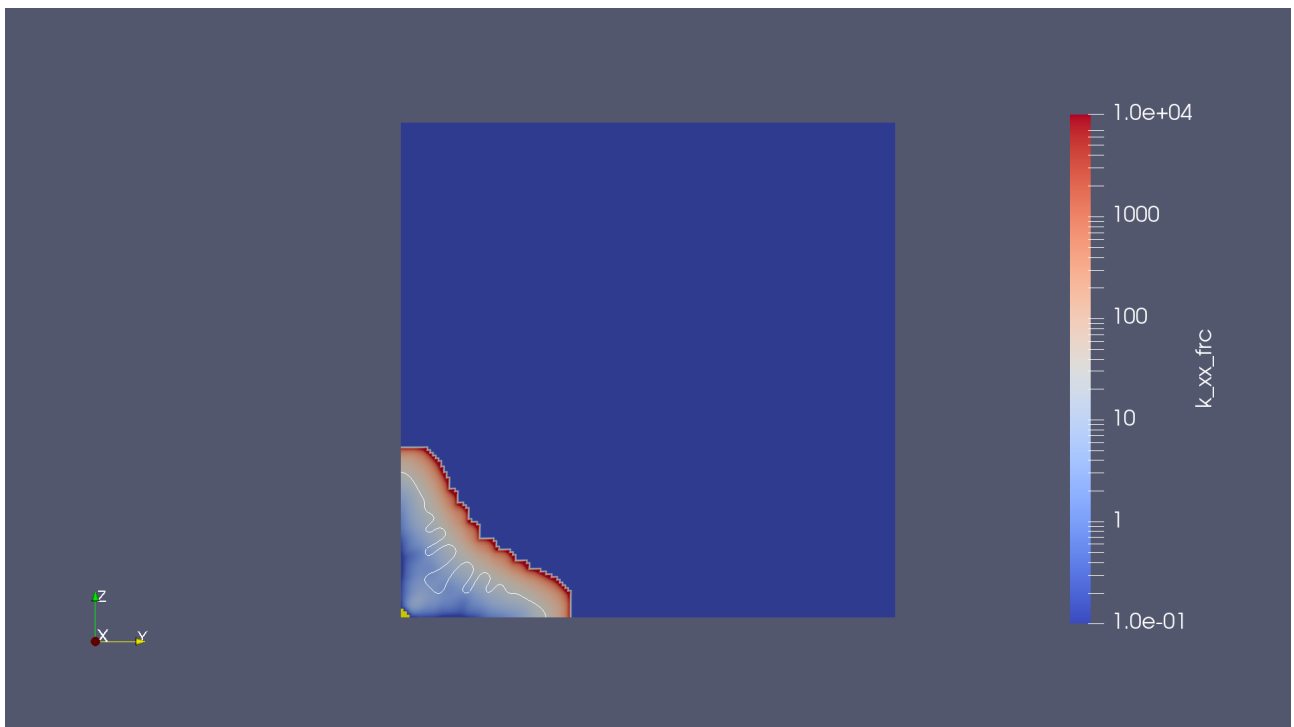


**Figure 15.** Visualisation in a slice in Paraview of  $k_{xx}$  obtained with the drag force for  $N^* = 0.1609$

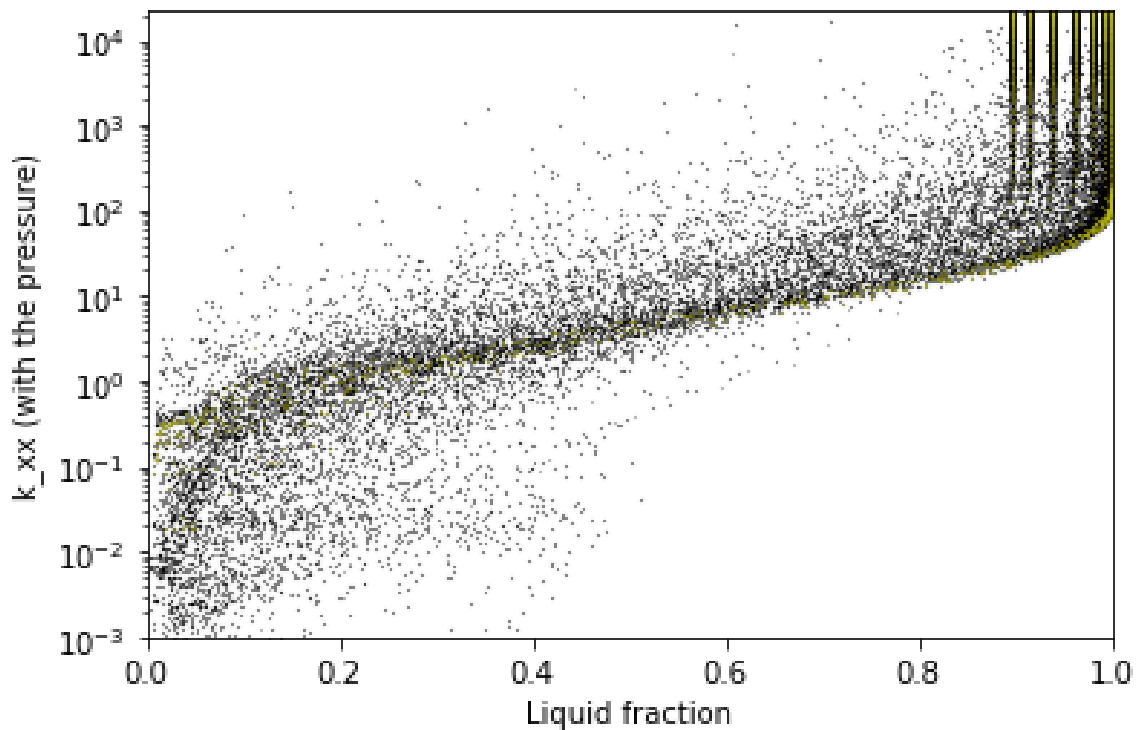


**Figure 16.** Evolution of the coefficient  $k_{xx\_pres}$  in terms of the liquid fraction for every points in the lattice for  $N^* = 0.0662$

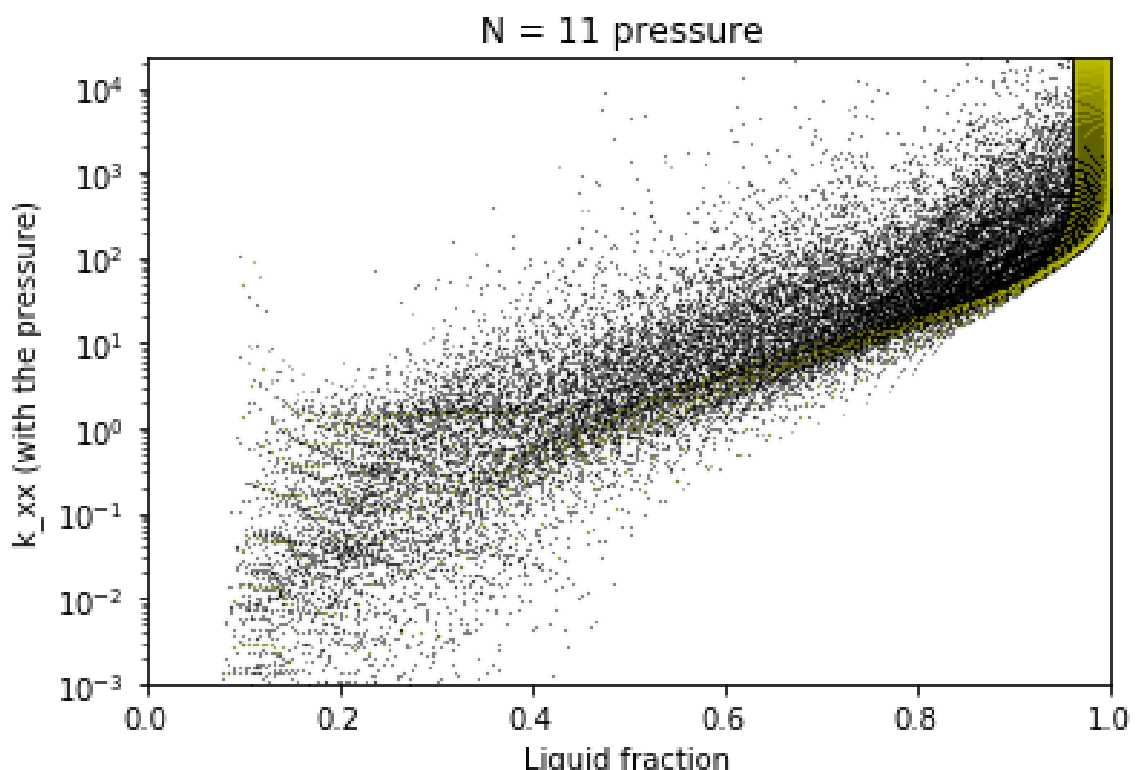


**Figure 17.** Evolution of the coefficient  $k_{xx\_pres}$  in terms of the liquid fraction for every points in the lattice for  $N^* = 0.1041$

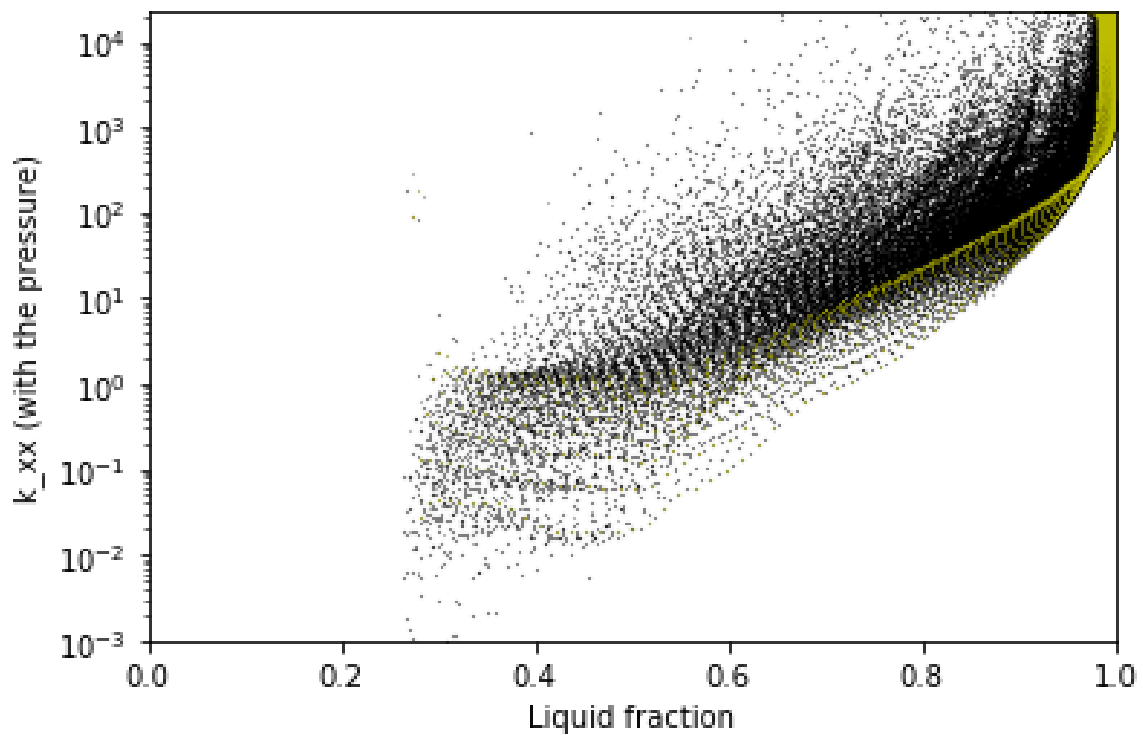


**Figure 18.** Evolution of the coefficient  $k_{xx\_pres}$  in terms of the liquid fraction for every points in the lattice for  $N^* = 0.1609$

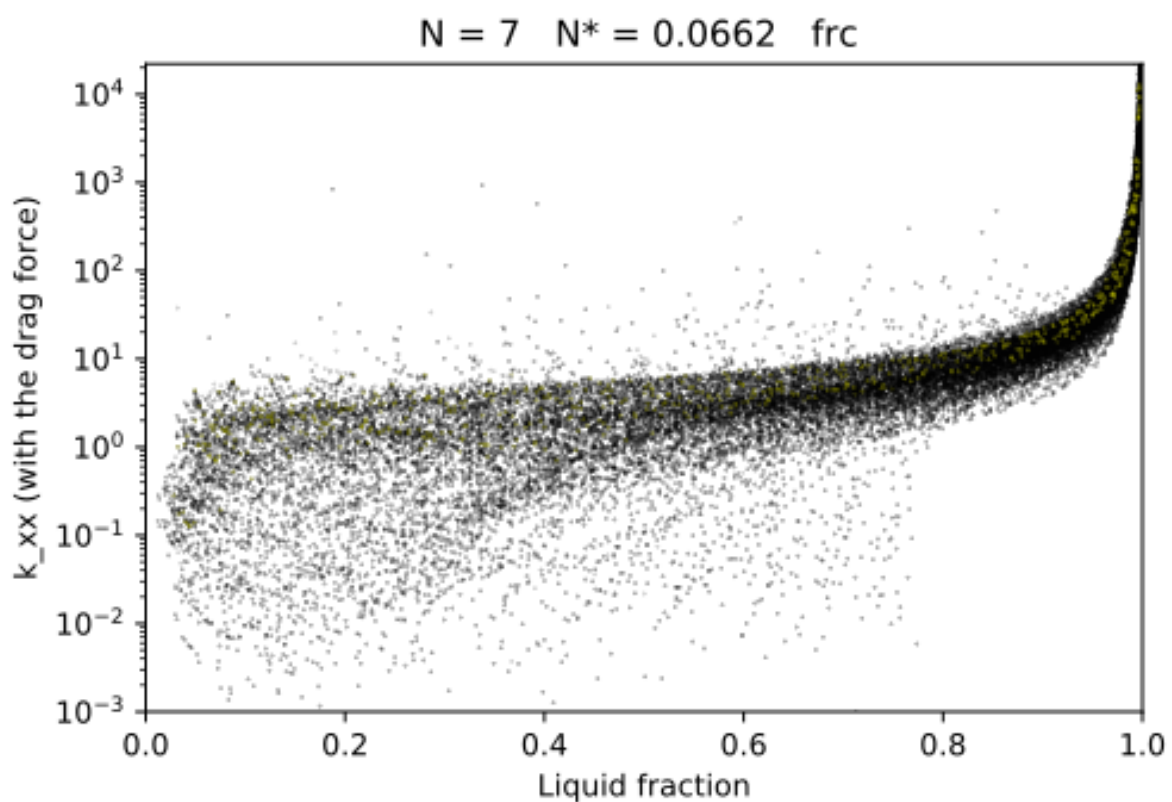


**Figure 19.** Evolution of the coefficient  $k_{xx\_frc}$  in terms of the liquid fraction for every points in the lattice for  $N^* = 0.0662$

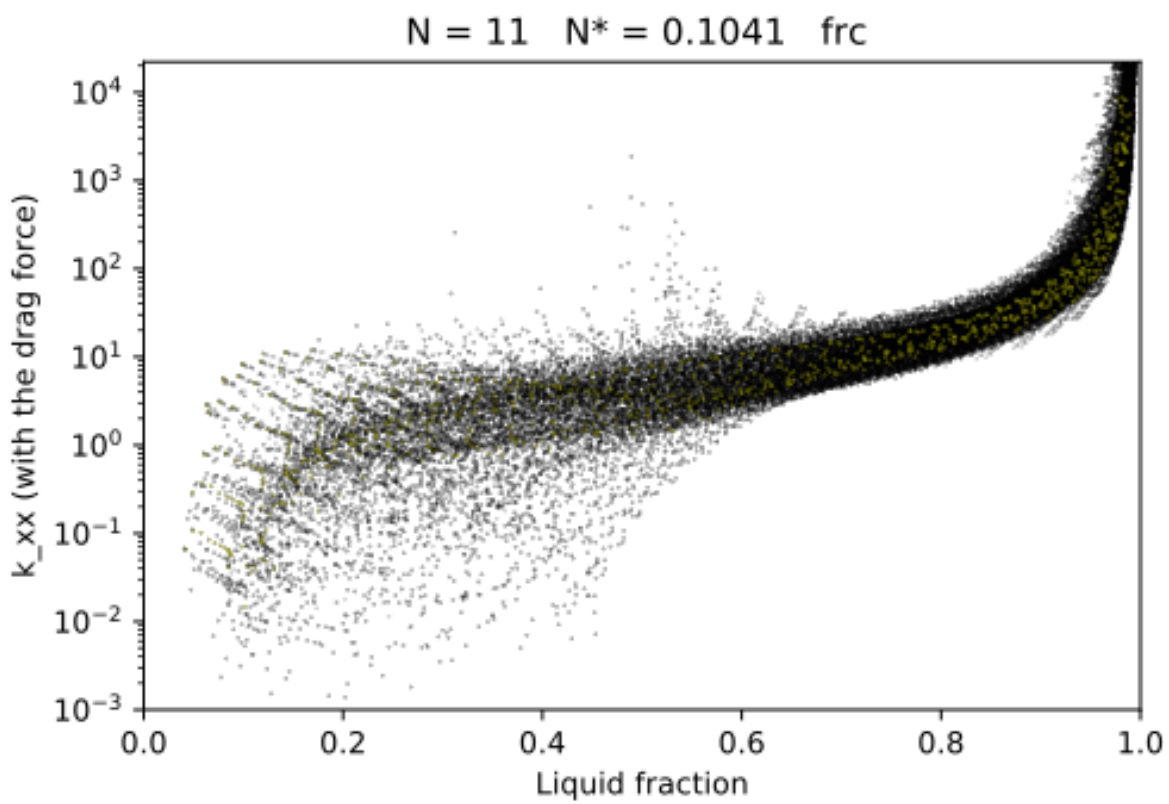


**Figure 20.** Evolution of the coefficient  $k_{xx\_frc}$  in terms of the liquid fraction for every points in the lattice for  $N^* = 0.1041$

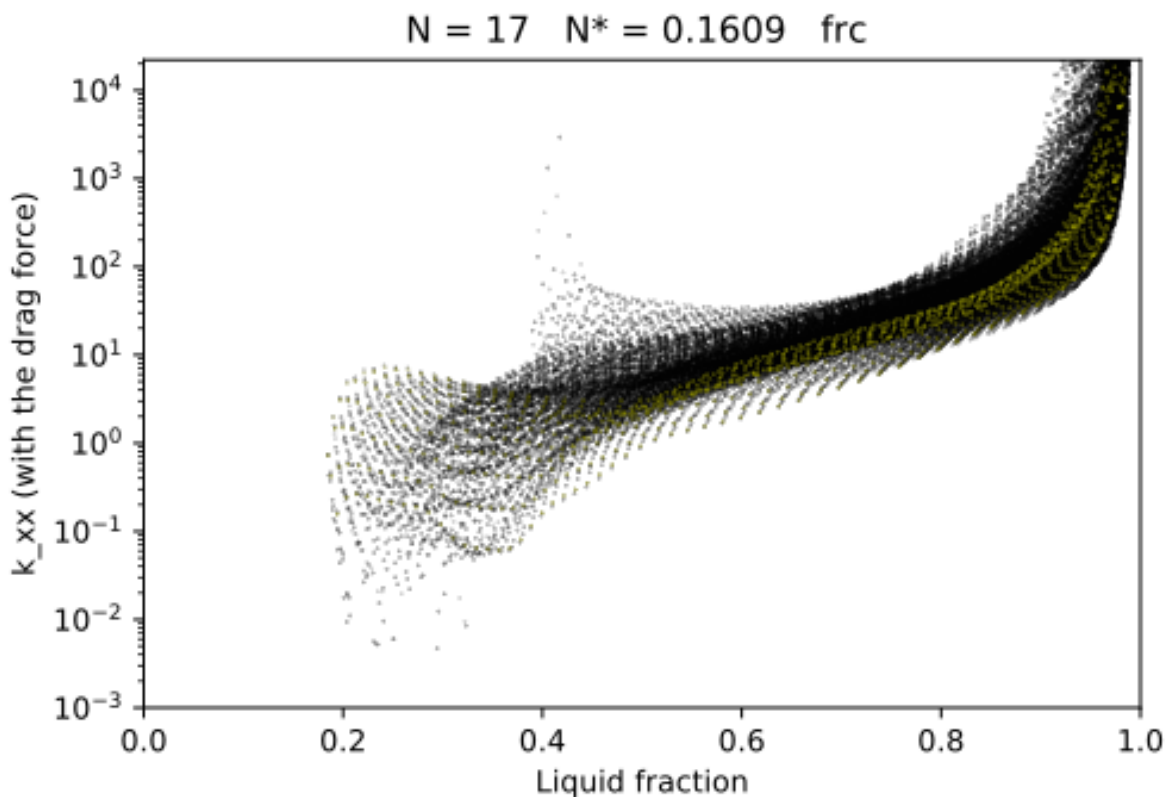


**Figure 21.** Evolution of the coefficient  $k_{xx\_frc}$  in terms of the liquid fraction for every points in the lattice for  $N^* = 0.1609$

As shown in Figure 16 and Figure 19, it can be seen that there is not a trustworthy permeability that can be obtained as the dots are really scattered for small sizes of representative elementary volume. Nevertheless, as shown in Figure 17 and Figure 20, the yellow curves seem to be precise and its dots seem to be aligned. That is precisely at this size of representative elementary volume that a permeability can then be defined. In these figures, it can be seen that there is only one yellow curve considering the fact that only the secondary branches of the dendrite are being averaged. Finally, Figure 18 and Figure 21 show the calculated permeability for each mesh dots in the simulation domain when the large scales are becoming to be averaged. In these figures, it can be seen that a second yellow curve appears as the primary branches and the secondary branches of the dendrite are averaged.

## 5 Conclusion

Thanks to numerical simulations using a Lattice Boltzmann Method, a model of confinement has been validated comparing it to analytical developments. A model of drag force for the case of dendrites with complex geometries has been established. This model of drag force takes into consideration the confinement with the coefficient  $k'$  whose evolution with the confinement  $\chi$  has been determined.

Furthermore, a study on the spatial distribution of the drag force has opened the doors to the development of a model of hydrodynamic permeability within the dendrites. To determine a permeability derived from Darcy's law, the fields calculated in the simulations have been averaged using a moving volume average. The size of this volume has been related to the sizes characterizing the dendrites morphology to estimate the proper size for a representative volume element. Through the use of both pressure and drag force distribution, a apparent permeability  $k_{xx}$  of the dendrites has been quantified and related to the local liquid volume fraction.

## Acknowledgements

High Performance Computing resources were provided by the EXPLOR centre hosted by the University de Lorraine.

## References

- [1] H. de Groh III, P. Weidman, R. Zakhem, S. Ahuja, and C. Beckermann. Calculation of dendrite settling velocities using a porous envelope. *Metallurgical Transactions B*, 24(5):749–753, 1993.
- [2] A. V. D Tourret, L Sturz and M. Založník3. Comparing mesoscopic models for dendritic growth. *Materials Science and Engineering*, 861, 2020.
- [3] A. S. Sangani and A. Acrivos. Slow flow through a periodic array of spheres. *Int. J. Multiphase Flow*, 8 (4):343–360, 1982.
- [4] A. Martin de Bazelaire. Etude numérique d'écoulement autour de géométries complexes. Technical report, Institut Jean Lamour, Université de Lorraine, 09 2020.
- [5] M. GISSELBRECHT. *Simulation des interactions hydrodynamiques entre inclusions dans un métal liquide : établissement de noyaux d'agrégation dans les conditions représentatives du procédé de flottation*. PhD thesis, Université de Lorraine, 2019.
- [6] M. Bouzidi, M. Firdaouss, and P. Lallemand. Momentum transfer of a boltzmann-lattice fluid with boundaries. *Physics of Fluids*, 13(11):3453–3459, 2001.
- [7] A. M. Roma, C. S. Peskin, and M. J. Berger. An adaptive version of the immersed boundary method. *Journal of Computational Physics*, 153:509—534, 1999.